Organic Electron Delocalization Modulated by Ligand Charge States in $[L_2M]^{n-}$ Complexes of Group 13 Ions

Amela Arnold, Tobias J. Sherbow, Richard I. Sayler, R. David Britt, Emily J. Thompson, M. Teresa Muñoz, James C. Fettinger, Louise A. Berben*

Department of Chemistry, University of California Davis, California 95616, USA

ABSTRACT: Water stable organic mixed valence (MV) compounds have been prepared by reaction of reduced bis(imino)pyridine ligands (I_2P) with the trichloride salts of Al, Ga, and In. Coordination of two tridentate ligands to each ion affords octahedral complexes that are accessible with five ligand charge states: $[(I_2P^0)(I_2P^-)M]^{2+}$, $[(I_2P^-)_2M]^+$, $(I_2P^-)(I_2P^{2-})M$, $[(I_2P^{2-})_2M]^-$, $[(I_2P^{2-})(I_2P^{3-})M]^{2-}$, and for M = Al only, $[(I_2P^{3-})_2M]^{3-}$. In solid-state structures the anionic members of the redox series are stabilized by intercalation of Na^+ cations within the ligands. The MV members of the redox series, $(I_2P^-)(I_2P^{2-})M$ and $[(I_2P^{2-})(I_2P^{3-})M]^{2-}$, show characteristic intervalence transitions, in the near-infrared region between 6800 - 7400 and 7800 – 9000 cm^{-1}, respectively. Cyclic voltammetry (CV), NIR spectroscopic, and X-ray structural studies support the assignment of Class II for compounds $[(I_2P^{2-})(I_2P^{3-})M]^{2-}$ and Class III for M = Al and Ga in $(I_2P^-)(I_2P^{2-})M$. All compounds containing a singly reduced I_2P^- ligand exhibit a sharp, low energy transition in the region 5100 – 5600 cm^{-1} that corresponds to a $\pi^* - \pi^*$ transition. CV studies demonstrate that the electron transfer events in each of the redox series, Al, Ga, and In span 2.2, 1.4 and 1.2 V, respectively.

INTRODUCTION

Mixed valent (MV) complexes are simple models with which to study electron delocalization and electron transfer and understand geometric and electronic effects that facilitate multi-electron redox processes in biological systems,[1] in materials,[2,3] and devices.[4,5,6] The degree of electron delocalization in an organic molecule is related to conductivity and so fundamental studies of electron delocalization in MV compounds can inform the design of organic molecular wires and devices.[7] The Robin and Day classification categorize delocalization of charge between two redox centers. Class I complexes have redox centers which do not measurably interact; Class II complexes have partially delocalized electrons; and Class III complexes are delocalized, and the two redox sites are indistinguishable.[8]

Model compounds used to study mixed-valency traditionally comprise transition element redox sites linked by organic bridges. The Creutz-Taube (CT) ion, with Ru atoms bridged by pyrazine, is the classic of these traditional models, and considered fully delocalized (Class III, Chart 1A).[9] A recent report highlighted metal-metal bonded clusters as an alternative topology to support Class II/III mixed valency in octahedral iron clusters where the extent of electron delocalization is modulated by capping ligands (Chart 1B).[10] Ongoing work with organic MV systems has also contributed to our understanding within the Robin and Day scheme, and highlights include radical cationic and anionic tertiary triarylamines,[11] and perchlorinated triphenylmethyl end groups,[12] joined by a variety of linkers (Chart 1C). Dimethoxybenzene has also served as end group.[13] Air-stable alkynyl- and alkynylphenyl-linked cyclic (aryl)(amino)carbenes, or "CAAC" radical cations have recently been reported to expand the scope of organic systems (Chart 1D).[8]

Chart 1. Topologies for mixed-valent models. Transition metal MV systems (A – B); organic MV systems (C – D).

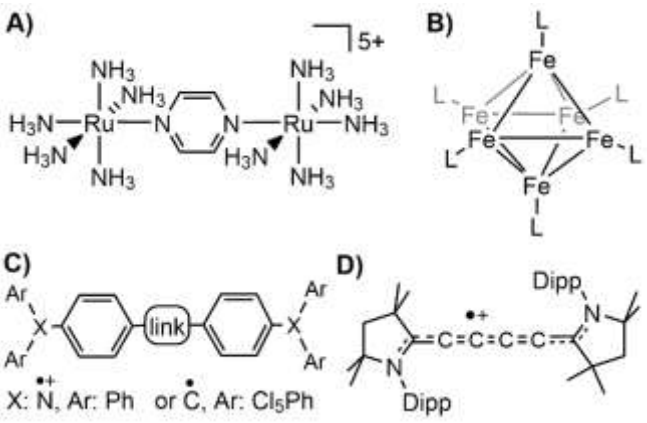

Common to the majority of highly delocalized MV systems are organic bridging linkers and end groups that can store one electron each. Redox-active ligand complexes of metal ions offer potentially high tunability where multiple electron transfers could be mediated at the organic end groups to give access to a redox series of strongly coupled states. These structures also have the potential to be tuned by synthetic modifications across a wide length scale. Traversing the series with one electron added at a time, every other member of an organic bis(ligand) charge series would be mixed-valent, and every other member would be either diamagnetic or biradical (Chart 2). Others have recognized the potential for rich electronic and magnetic properties if such systems could be realized and

reports of synthetic, structural and magnetic advances have appeared so that a number of localized Class I and partially delocalized Class II MV compounds exist, in which either transition elements,[14,15,16] or Group 13 ions,[17,18] link organic redox-active ligand end groups. Class III delocalization between redox active organic end groups has been achieved with square planar d^8 metal complexes,[19] and in each of those prior examples, the electronic properties of just one mixed-valent state were characterized.

Chart 2. Variable charge states of redox active ligands storing 0 - 3 electrons each. MV: mixed valent.

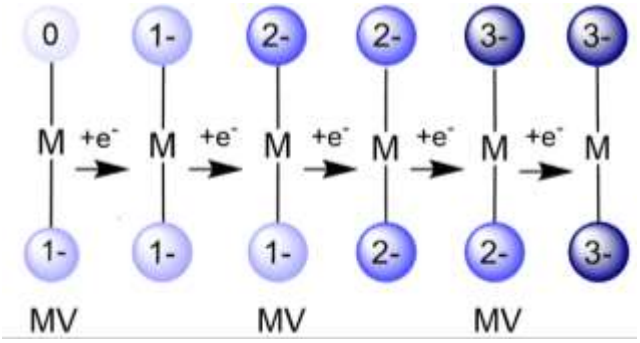

In this report we use structural, electrochemical, and spectroscopic characterization to ask which factors, including metal identity, geometry of the complexes, and the charge state in each series of complex, are important in determining the magnitude of electronic coupling between ligands. We uncover a suitable topology to support delocalized and tunable Class II, Class II/III, and Class III systems (Scheme 1). We characterize three separate ligand charge series, containing Al, Ga, and In central ions over five ligand-based charge states, and where three of the five members of each charge series are MV (Chart 2). Within a single ligand of 1- charge, $\pi^* - \pi^*$ transitions are observed and the inter-ligand delocalization varies with metal ion and with ligand charge: Class III behavior is most readily obtained for Al and Ga when ligands have 1-/2- charge and Class II/III behavior for charge states 2-/3-. These results enhance our understanding of spin interactions in organic radicals which has ongoing relevance to molecular electronics and to quantum information processes.

Scheme 1. Effect on delocalization as a result of varying Group 13 metal or charge state of ligand.

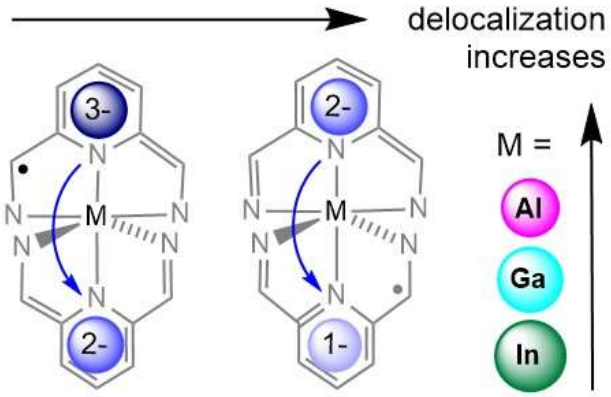

RESULTS AND DISCUSSION

Synthesis of Complexes. A series of complexes with two tridentate ligands $(I_2P)_2M$, where M = Al, Ga and In, were synthesized (I_2P is 2,6-Bis{1-[(2-methoxyphenyl)imino]-benzyl}pyridine, Scheme 2 where the labels **a**, **b**, and **c** throughout the text denote Al, Ga, and In complexes, respectively). Complexes **1** are MV $[(I_2P)(I_2P^{-})M]^{2+}$, complexes **2** are biradical $[(I_2P^{-})_2M]^{+}$, complexes **3** are MV and neutral $[(I_2P^{-})(I_2P^{2-})M]$, complexes **4** are diamagnetic $[(I_2P^{2-})_2M]^{-}$, **5** are MV $[(I_2P^{2-})(I_2P^{3-})M]^{2-}$, and **6** was only accessed for Al, $[(I_2P^{3-})_2Al]^{3-}$. The singly-ligated complex $(I_2P^{-})AlCl_2$ (**7**) was prepared by a similar method to that previously described (Scheme 2, see SI for details).[20]

Scheme 2. Syntheses of complexes 1 – 4, 6a and 7. Ligand charge states denoted in blue.

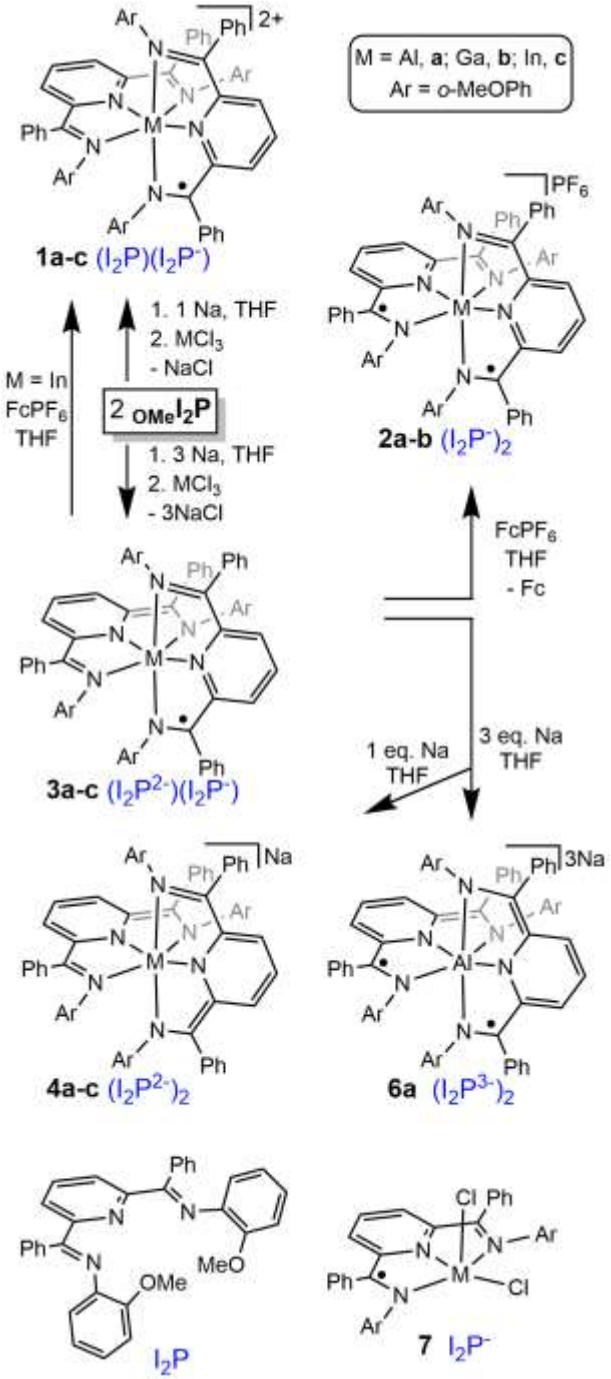

Mixed-valent compounds **3** were the most straightforward of the charge series to prepare, and many of the other compounds **1** – **6** were subsequently prepared by either oxidation or reduction of complexes **3** (Scheme 2). Reaction of two equivalents of I_2P with three equivalents of Na in THF solution over 24 h gave a dark burgundy solution. The metal chloride MCl_3 was dissolved in THF and added to the reduced ligand to afford a deep red solution for all three complexes **3a** – **c**. Following workup, red-brown **3a** – **c** were isolated in 86, 53, and 38 % yield, respectively, and characterized using high resolution mass spectrometry (HRMS), single crystal X-ray diffraction (XRD), UV-Vis-NIR absorption spectroscopy, electron paramagnetic resonance spectroscopy (EPR), combustion analyses, and the Evan's method which indicated that μ_{eff} = 1.90, 1.94, and 1.75 μ_B, respectively, consistent with one unpaired electron on each complex. The XRD, UV-Vis-NIR, and EPR analyses are described in greater detail below.

Complexes $[(I_2P^{\cdot})(I_2P)Al][AlCl_4]_2$ (**1a**) and $[(I_2P^{\cdot})(I_2P)Ga][GaCl_4]_2$ (**1b**) were obtained by reduction of two equivalents of I_2P with one equivalent of sodium followed by three equivalents of either $AlCl_3$ or $GaCl_3$ in THF solution. Red paramagnetic solids were isolated in 15 and 51 % yield, respectively, and have magnetic moment, μ_{eff} = 1.53, and 1.85 μ_B. Complex $[(I_2P^{\cdot})(I_2P)In][Na][PF_6]_3$ (**1c**) was isolated from a reaction of I_2P with one equivalent of sodium and subsequent addition of $InCl_3$ and KPF_6 in THF. Red crystals of **1c** were obtained in 11% yield and have μ_{eff} = 2.05 μ_B. We also obtained **1c** in 13 % yield by oxidation of **3c** with one equivalent of $FcPF_6$. The one-electron oxidized product from a reaction of **3c** should be **2c** but none of that was observed. Complexes **1a** – **c** were also characterized by XRD, combustion analysis, and UV-Vis-NIR absorption spectroscopy.

Compounds $[(I_2P^{\cdot})_2Al][PF_6]$ (**2a**) and $[(I_2P^{\cdot})_2Ga][PF_6]$ (**2b**) were obtained in 86 and 23 % yield, respectively, by oxidation of **3a** and **3b**, using 1 equivalent of $FcPF_6$ in THF (Scheme 1). Compound **2b** could alternatively be obtained in 65 % yield after reaction of $GaCl_3$ and KPF_6 with $Na_2[I_2P^{\cdot}]_2$. Attempts to produce **2c** via either of these routes were unsuccessful; the resulting product was predominantly **1c**. Characterization of **2a** and **2b** was achieved using HRMS, XRD, and EPR spectroscopy. The magnetic moments of the compounds are 2.80 and 3.00 μ_B, respectively.

Diamagnetic **4a** – **c** were obtained in 86, 78, and 58 % yield, respectively. Syntheses of **4a** and **4b** were achieved via reduction of **3a** or **3b** with one equivalent of Na metal in THF solution. Reduction of two equivalents of I_2P with four equivalents of sodium in THF, and subsequent addition of $InCl_3$ in THF afforded $[(I_2P^{-2})_2In][Na]$ (**4c**). The proton NMR spectra of each of **4a** – **c** are consistent with two-electron reduced I_2P ligands. For example, a doublet of doublets for the *p*-pyridine proton resonance is observed at 5.39, 5.53, and 5.59 ppm for **4a**, **4b**, and **4c**, respectively (Figures S1, S2, S3). Solid samples of **4a** and **4b** decompose in a nitrogen-filled glovebox over 24 and 72 hours, respectively, whereas a solid sample of **4c** was stable for at least 7 days.

Complexes **5**, with I_2P^{2-} and I_2P^{3-} ligands, could not be isolated and their spectroscopic properties are described in a later section where **5a** – **c** are generated in situ from **3a** – **c**. Complex **6a** was synthesized by reduction of **3a** with 3.3 equiv. of Na in THF to give a dark brown color over 4 hr at room temperature. The trianionic charge state of I_2P has only rarely been isolated,[21] and we know of no other compound containing two I_2P^{3-} ligands. Single crystals of **6a** were isolated as brown-black blocks grown at -20 °C from THF (65 % yield). XRD was employed to identify **6a** at low temperature but its thermal instability (decomposition in less than three minutes at 25°C) thwarted further characterization.

UV-Vis spectra of the redox series show an increase in the extinction coefficients (ε, L $mol^{-1}cm^{-1}$) and a shift to lower energy, as the ligand is further reduced (Figure S4). Using the Al series as an example: ε = 5010 $Lmol^{-1}cm^{-1}$ for **1a** at 403 nm, 12200 for **2a** at 450, 17300 for **3a** at 457, 19500 for **4a** at 476. Similar trends were observed in the Ga and In redox series, and all of these bands are assigned as π - π* transitions. As the ligands are further reduced, the shift to lower energy implies a smaller π - π* energy gap. A similar trend in the redox series of $[Co(tpy)_2]^{2+}$, $[Co(tpy)_2]^{+}$ and $[Co(tpy)_2]$ was observed where bands were observed at 387, 435 and 442 nm, respectively, as tpy ligands are further reduced (tpy = terpyridine).[16c]

Solid State Structures. Solid-state structures of the complexes **1a** – **c**, **2a** – **b**, **3a** – **c**, **4b** – **c** and **6a** were obtained from single crystals using X-ray diffraction. Experimental details of the crystal growth, data collection and refinement, along with comprehensive tables of bond lengths and angles are available in the Supporting Information (Tables S1 - S6, Chart S1). Based on previous studies of I_2P complexes, bond lengths obtained from solid-state structures are valuable metrics for assignment of ligand charge state (Chart 3).[22,23] In neutral ligands the imino C–N bond length is 1.28 – 1.32 Å, and upon one-electron reduction, a C–N bond elongates to 1.32 – 1.34 Å on one side only.[17a-c] When a one-electron reduction is delocalized over the entire ligand then bond lengths have intermediate length around 1.32 Å. When a two-electron reduction is localized at the imino group, observed bond lengths range from 1.41 – 1.45 Å.[23] If the one- or two-electron reduction events are not localized at one of the imino functional groups, the added electrons are often delocalized throughout the ligand framework.[20,24]

Chart 3. C–N and M–N bond length designations used throughout the text. im = imine, am = amine.

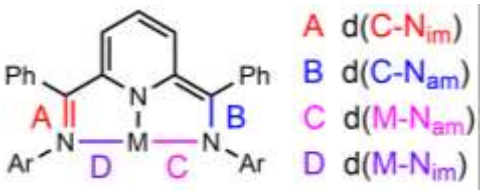

Complexes **1a** – **c** each contain one neutral and one singly reduced ligand (Figure S5, Table 1), and **1a** – **b** are pseudo-octahedral, with Npy-M-Npy′ bond angles of 175.40(12)° and 178.7(1)°. The I_2P and $I_2P^{\cdot}$ ligands in **1a** have C—N bond lengths 1.303(4), 1.305(4) Å, and 1.316(4) and 1.322(4) Å, respectively. In **1b**, the C—N bond lengths in I_2P and $I_2P^{\cdot}$ are 1.286(4) and 1.298(4) Å, 1.321(4) and 1.323(4) Å, respectively (Table 1). The mirror symmetry of the anionic ligands in **1a** and **1b** suggests that the radical electron is highly delocalized within the $I_2P^{\cdot}$ framework, but no

evidence for interligand delocalization was observed. Eight coordinate **1c** is bicapped trigonal prismatic with six *N*-donor atoms from I_2P ligands, and two *O*-donor atoms from *o*-methoxyaniline (Figure S5). One ligand of **1c** is generated by symmetry and the two averaged C—N bond lengths are 1.291(8) and 1.329(7) Å. The two In—O distances are also symmetry equivalent and are 2.818(4) Å and similar to the In-O distances observed with crown ether ligands (2.620(2) – 2.842(2) Å),[25] and with solvate interactions such as with THF (for example, 2.725(3) and 2.732(3) Å).[26,27] A *trans* influence is noted where the In—N_{am} bond *trans* to the *o*-methoxyaniline is 0.138(5) Å longer than the other In—N_{am} bond in **1c**.

Table 1. Selected bond lengths discussed in the text. im = imine, am = amine.

C—N_{im} / C—N_{am} (Å)		
1a	1b	1c [a]
1.303(4)	1.321(4)	1.329(7)
1.305(4)	1.323(4)	1.291(8)
1.322(4)	1.286(4)	
1.316(4)	1.298(4)	
2a	2b	7
1.324(6)	1.322(6)	1.319(2)
1.314(7)	1.306(6)	1.328(2)
1.321(6)	1.320(6)	
1.322(6)	1.309(6)	
3a	3b	**3c**/**3c**′ average
1.318(4)	1.295(7)	1.291(9)
1.341(4)	1.331(7)	1.352(9)
1.352(4)	1.375(7)	1.293(9)
1.362(4)	1.327(7)	1.408(9)
6		4c [a]
1.409(5)		1.301(2)
1.383(4)		1.452(5)
1.409(5)		
1.383(4)		

[a] The asymmetric unit contains half of the molecule; the remaining bond lengths are generated by crystallographically -imposed symmetry.

Compounds **2a** and **2b** contain two singly reduced tridentate I_2P^- ligands and have overall 1+ charge (Figure S6). Each complex approximates octahedral and N_{py}-M-N_{py}′ angles are 179.29(17) and 178.75(16)°, respectively. The C—N bonds fall within a narrow range: 1.314(7) - 1.324(6) Å for **2a**, and 1.306(6) - 1.322(6) Å for **2b** (Table 1). Considering the M—N, C—N, and C—C bond lengths in these structures, they are best described as having a fully delocalized radical electron on each ligand.

Complexes **3a** – **c** have I_2P^- and I_2P^{2-} ligands (Figure 1, Chart 4). **3a** and **3b** can best be described as pseudo-octahedral and **3c** is an eight-coordinate, distorted bicapped trigonal prismatic geometry as in **1c** (Figure S5). The structure of **3c** contains two molecules in the asymmetric unit, with similar bond lengths and so this discussion uses average values. The bond angles around the In center in the distinct In molecules differ due to a benzene solvate associated with just one of the molecules. In all three of **3a** – **c**, the added electron on the singly-reduced ligand can be considered localized at the C atom of one imino functional group because C—N bond distances are quite different on each side of the ligand, as are Al—N bonds (Chart 4, Table 1). The electronic character of the I_2P^{2-} ligands in **3a** – **c** show some variation. In **3a**, I_2P^{2-} is symmetric with C—N bonds 1.362(4) and 1.352(4) Å, as in square planar complexes such as ($^{Ph}I_2P^{2-}$)AlCl.[28] In **3c**, I_2P^{2-} is asymmetric with localization of the added electron on one imino and the pyridyl donor. An intermediate structure is observed for **3b** where C—N bonds are 1.375(7) and 1.327(7) Å.

Single crystal X-ray analyses also confirmed the structures of **4b** and **4c**, in which both ligands have 2-charge (Figures S7, Table S5, S6). We were unable to crystallize **4a**, and the data for **4b** is of low quality. The C—N bond lengths in **4c** are 1.301(2) Å and 1.452(5), and these illustrate an asymmetric geometry (Table 1). Singly ligated **7** was also characterized crystallographically and C—N bond lengths are similar to those observed in **2a**: 1.319(2) and 1.328(2) Å (Figure S8, Table S4).

Complex **6** features two ligands that are each trianionic I_2P^{3-} (Figure 2, Tables S1, S4). Three Na^+ cations occupy two different environments, and all are coordinated to the ligands presumably stabilizing the highly reduced states. The Al—N_{im} bond lengths are surprisingly long, 2.100(3) and 2.087(3) Å, considering the 3- ligand charge state, and this is presumably due to involvement of ligand donor atoms in coordination to Na^+ ions. For comparison, the corresponding bonds in **3a** are 2.104(3) and 2.039(3) Å. The C—N_{im} bond lengths of I_2P^{3-} are 1.409(5) and 1.383(4) Å which we label as single bonds (Table 1).

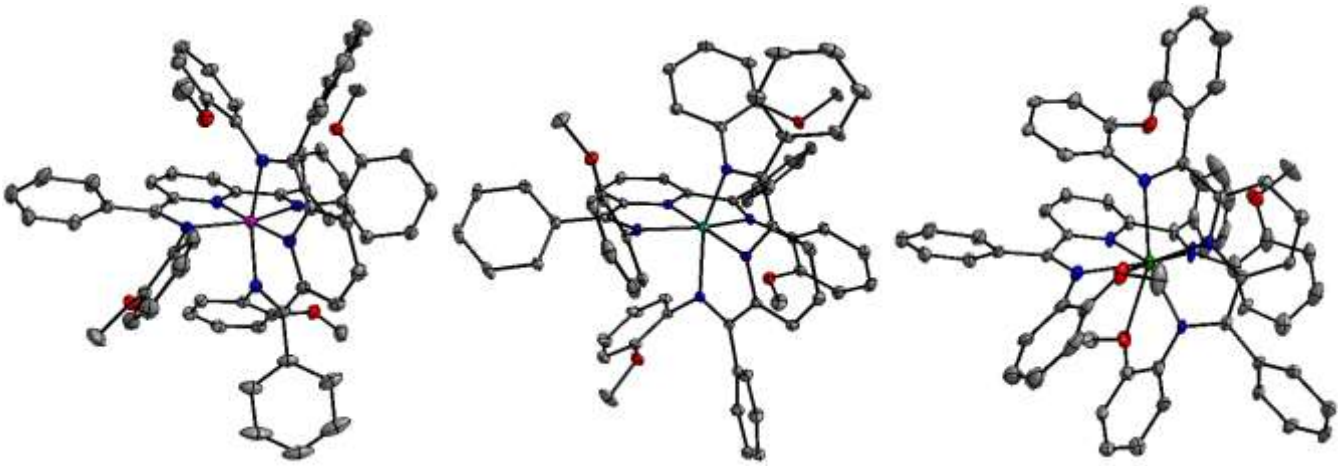

Figure 1. Solid-state crystal structures for (I_2P^-)(I_2P^{2-})Al in **3a**, (I_2P^-)(I_2P^{2-})Ga in **3b**, and (I_2P^-)(I_2P^{2-})In in **3c**. Pink, light blue, green, red, blue and grey ellipsoids represent Al, Ga, In, O, N, and C atoms, respectively. Ellipsoids are shown at 30% probability. Solvent molecules and hydrogen atoms omitted for clarity.

Chart 4. Selected bond lengths of 3a, 3b, and 3c.

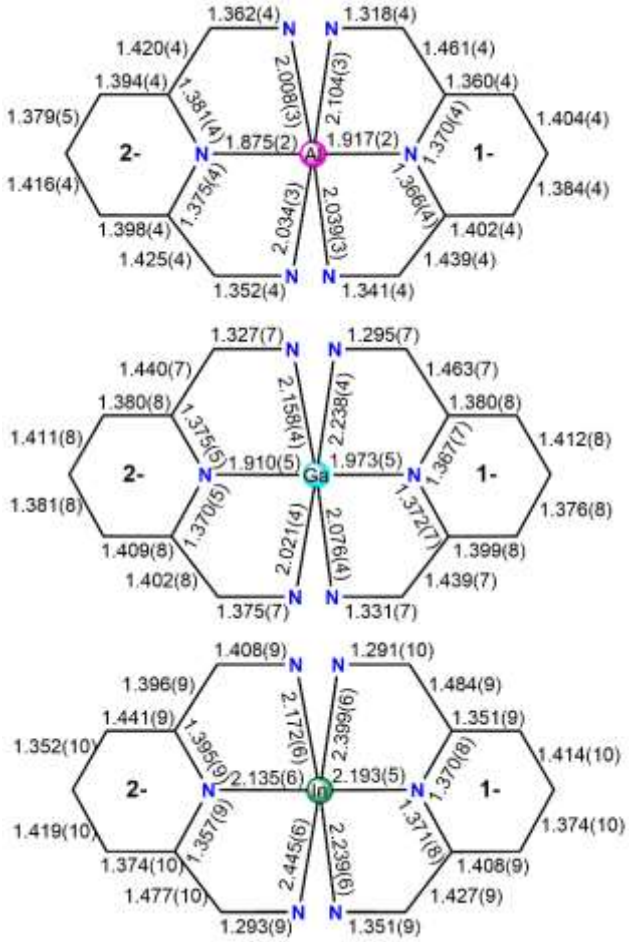

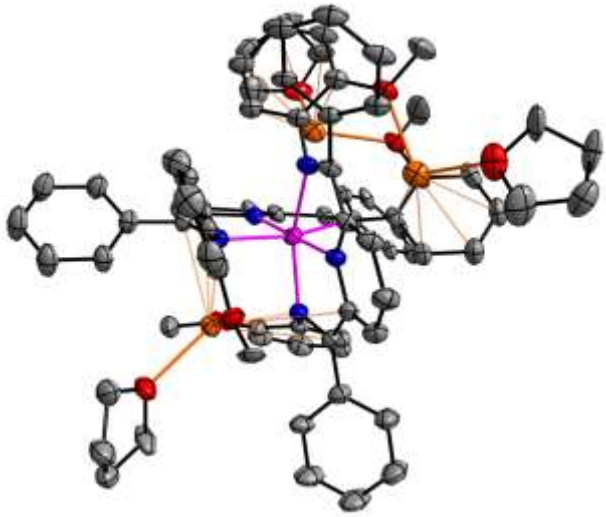

Figure 2. Solid state structure of [(I_2P^{3-})$_2$Al][NaTHF]$_3$ in **6a**. Pink, red, blue, orange and grey ellipsoids represent Al, O, N, Na, and C atoms, respectively. Ellipsoids shown at 30% probability level. Hydrogen atoms and most solvates omitted.

In each of the structurally characterized MV compounds, **1a – c**, and **3a – c**, comparison of the C—N bond lengths is effective using histograms to understand structural effects arising from electron delocalization (Figure 3).[16a] On the left side of each plot are the two shortest C—N bond lengths and on the right side the longest C—N bond length of each compound. These plots highlight how different or similar the C—N bond lengths are in each complex, and how these differences change between the Al, Ga, and In compounds. For complexes **1a – c**, the shortest C—N bonds are in neutral I_2P, the longest are both in I_2P^-, and both ligands are quite symmetric with mirror plane through the py ring. Comparison of **1a**, **1b**, and **1c** shows the greatest similarity between ligands' C—N bond lengths for **1a** > **1b** > **1c**. In **2a** and **7**, the C—N bond lengths are all nearly equivalent, and in **2b**, the radical is slightly more localized on one side of each ligand (Figure S9). In **3a** – **c**, the four C—N bond lengths are closer to equivalent

in **3a** than in **3b** than in **3c**, with **3a** approaching completely symmetric.

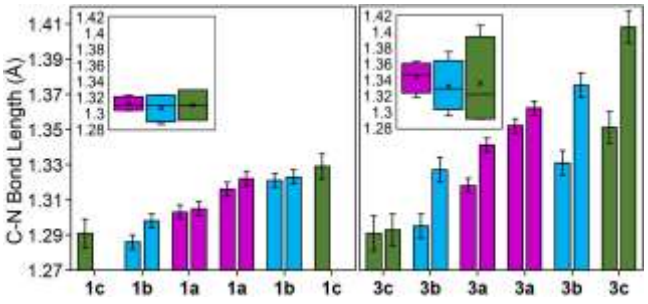

Figure 3. Shortest and longest C—N bond distances on left and right, respectively (Å, esd is error bars), for **1a – c** (left), and **3a – c** (right). Inset: X is average, and horizontal line is median C—N bond length; boxes span upper and lower quartiles. Al, pink; Ga, blue; and In, green.

Electrochemical Studies. Cyclic voltammograms (CVs) of **3a – c** were acquired in a 0.1 M Bu_4NBF_4 MeCN solution, and display redox events spanning at least five ligand-based charge states from $[(I_2P)(I_2P^{-})M]^{2+}$ up to $[(I_2P^{2-})(I_2P^{3-})M]^{2-}$ (Figure 4, Table 2). As an example, the CV of **3a** showed reversible redox couples at 0.06, -0.31, -1.09, and -1.53 V vs. SCE corresponding to the $\mathbf{3a}^{2+/+}$, $\mathbf{3a}^{+/0}$, $\mathbf{3a}^{0/-}$, and $\mathbf{3a}^{-/2-}$ couples, respectively (Figure 4, Table 2). A fifth irreversible reduction at -2.12 V is attributed to the $\mathbf{3a}^{2-/3-}$ redox couple. The $\mathbf{3}^{0/-}$ couples in each complex are observed at very similar potentials for **3b** and **3c**, and then subsequent reduction and oxidation events are spaced more closely for **3b** and **3c**. The final $\mathbf{3}^{2-/3-}$ couple is not present in **3b** and **3c** (Figure S10). Previous work by Wieghardt and coworkers described $[(I_2P)_2Zn]^{2+}$,[16b] and in that study, reversible ligand-based redox events at $E_{½}$ = -0.9 and -1.26 V vs SCE were assigned as $[(I_2P)_2Zn^{II}]^{2+}/[(I_2P)(I_2P^{-})Zn^{II}]^{+}$, and $[(I_2P)(I_2P^{-})Zn^{II}]^{+}/[(I_2P^{-})_2Zn^{II}]$ couples. These events are spaced similarly by 280 mV. However, the potential for ligand reduction at equal ligand charge level is about 1.32 V more negative for I_2P on Zn^{2+} than for I_2P stabilized by Group 13 cations.

Table 2. Formal potentials ($E_{1/2}$), and peak-to-peak potentials (ΔE_p), for 3a – c obtained from CVs in 0.1 M Bu_4NBF_4 MeCN.

	$E_{1/2}$ (V vs. SCE)			ΔE_p		
	3a	3b	3c	3a	3b	3c
$\mathbf{3}^{2+/1+}$	0.06	-0.02	-0.15	72	58	65
$\mathbf{3}^{1+/0}$	-0.30	-0.34	-0.48	72	41	78
$\mathbf{3}^{0/1-}$	-1.08	-1.06	-1.08	58	41	84
$\mathbf{3}^{1-/2-}$	-1.51	-1.44	-1.36	72	56	64
$\mathbf{3}^{2-/3-}$	-2.12			125		
$\Delta\Delta E_{1/2}$	2.18	1.42	1.21			

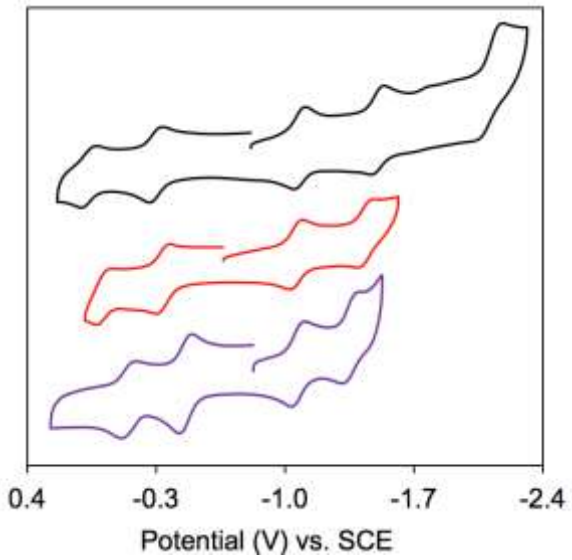

Figure 4. CVs of complexes **3a**, black; **3b**, red; and **3c**, purple. Collected in 0.1 M Bu_4NBF_4 MeCN with a glassy carbon working electrode at 0.1 V s^{-1}.

The formal potentials ($E_{½}$) for reversible redox couples for complexes **3a – c** span 1.57 V, 1.42 V and 1.21 V, respectively, indicating that electrons can be stored over a wide potential window. Electrochemical experiments performed on **3a** in 0.1 M Bu_4NBF_4 MeCN/H_2O (90:10) and **3b** in 0.1M KPF_6 MeCN/H_2O (15:85) revealed CV's comparable to those recorded in MeCN albeit with smaller solvent window that precluded observation of the $\mathbf{3a}^{2-/3-}$ couple. CV's recorded for **3a** after 3 hours in this solution revealed little change and after 21 hours, about 50% of the original CV signal remained (Figure S11). Aqueous stability is unusual for an Al(III) complex since formation of $[Al(H_2O)_x(OH)_y]^{3-y}$ is facile.[29] Here the tridentate ligands and coordinative saturation of the Al center hinder the reactions of Al(III) with water. We have previously shown that $(^{Ph}I_2P^{2-})AlH$ reacts with water to afford the alumoxanes, $[(^{Ph}HI_2P^{-})AlH]_2(\mu\text{-}O)$ or $[(^{Ph}HI_2P^{-})Al(OH)]_2(\mu\text{-}O)$,[30] and that $(I_2P^{2-})AlCl$ reacts with organic acids in THF solution,[23b] and it is likely that a similar ligand protonation event initiates slow decomposition of **3a** and **3b** in the present example.

Determination of Comproportionation Constants. Neutral complexes **3a – c** were used for analysis of electron transfer properties by cyclic voltammetry (CV). To ensure that each of the observed redox events are reversible, we performed variable scan rate experiments and constructed plots of current versus sqrt scan rate according to equation S1 (Figure S12).

Electrochemical data were also collected for **3a – c** in the lower dielectric constant solvent, THF (ε = 7.58), and for **3a** in propylene carbonate (PC, ε = 64) so that the spacing between successive redox couples ($\Delta E_{½}$) could be assessed over a range of dielectric constant solvents, Δε = 29 - 56. We observed that $\Delta E_{½}$ is not affected significantly by ion-pairing or Coulombic/electrostatic effects (Table S7, S8). The range Δε = 29 has been used by others to draw similar conclusions.[10] For such a dielectric range, Coulombic effects should produce much larger effects (100+ mV) to the $\Delta E_{½}$ than the ones observed here (0 - 30 mV).[31]

Calculation of comproportionation equilibrium constants (K_c), which can guide a description of the stability of each charge state relative to disproportionation. These values give the first indication as to the extent of interaction between redox centers in MV species. As a point of reference, the Class III Creutz-Taube ion has a $K_c = 10^{7.3}$ in acetonitrile, determined by electrochemical data.[32] K_c values were calculated from the distances between successive $E_{1/2}$ values using equation S2. For each of the complexes K_c values across the electron transfer series are greatest for $(I_2P^{\cdot-})(I_2P^{2-})M$, whose comproportionation reaction is shown in equation 1:

$$(I_2P^{\cdot-})_2M + (I_2P^{2-})_2M \rightleftarrows 2(I_2P^{\cdot-})(I_2P^{2-})M \qquad \text{eqn 1}$$

These values span 10^{10} to 10^{13} and suggest Class III mixed-valency for **3a** – **c** (Table 3). The greatest electronic coupling, is mediated by Al ($K_c = 10^{13}$), relative to Ga ($K_c = 10^{12}$), and In ($K_c = 10^{10}$). Measured K_c values for $(I_2P^{\cdot-})_2M$ (**3**$^{+}$, equivalent to **2a** – **c**), and $(I_2P^{2-})_2M$ (**3**$^{-}$, equivalent to **4a** - **c**) are roughly six orders of magnitude lower than those observed for **3a** – **c**, suggesting there is increased stability for the MV complex. When K_c values are obtained from CV data acquired in 0.3 M Bu_4NPF_6 THF for **3a** – **3c**, or 0.1 M Bu_4NBF_4 PC solution for **3a** very similar results were obtained. (Table S8-S9, Figure S13). Lack of solvent dependence further suggests Class III mixed valency for **3a** – **c**.[29,8] Fully reversible redox events were not accessible to allow determination of K_c for $(I_2P)(I_2P^{\cdot-})_2M$ (**3**$^{2+}$, equivalent to **1a** – **c**) or $(I_2P^{2-})(I_2P^{3-})_2M$ (**3**$^{2-}$, equivalent to **5a** – **c**).

Table 3. K_c values for 3^{+}, 3, and 3^{-}, obtained from CV data collected in 0.1 M Bu_4NPF_6 MeCN.

		3a K_c ($\Delta E_{1/2}$)	**3b** K_c ($\Delta E_{1/2}$)	**3c** K_c ($\Delta E_{1/2}$)
$(I_2P^{\cdot-})_2M$	**3**$^{+}$	1.3×10^6 (0.36 V)	3.3×10^5 (0.33 V)	2.7×10^5 (0.32 V)
$(I_2P^{\cdot-})(I_2P^{2-})M$	**3**	1.8×10^{13} (0.78 V)	1.6×10^{12} (0.72 V)	2.0×10^{10} (0.61 V)
$(I_2P^{2-})_2M$	**3**$^{-}$	1.6×10^7 (0.43 V)	2.2×10^6 (0.38 V)	4.0×10^4 (0.27 V)

Absorption Spectra. To further understand delocalization in MV metal complexes, an analysis of the intervalence charge transfer bands is generally performed on absorption bands observed in the near infra-red (NIR) region of the optical spectrum. In this work we refer to observed charge transfer bands in the Class II systems as ligand-ligand charge transfer (LLCT), so as to readily differentiate from the intraligand π* - π* transitions. Low energy absorption bands were observed in the NIR for complexes **1a** – **c**, **2a** – **b**, **3a** – **c**, and **5a** – **c** (Figure 5), and these bands are plotted as reduced absorption (ε/ν) versus ν to provide a more accurate estimation of ν_{max}.[33]

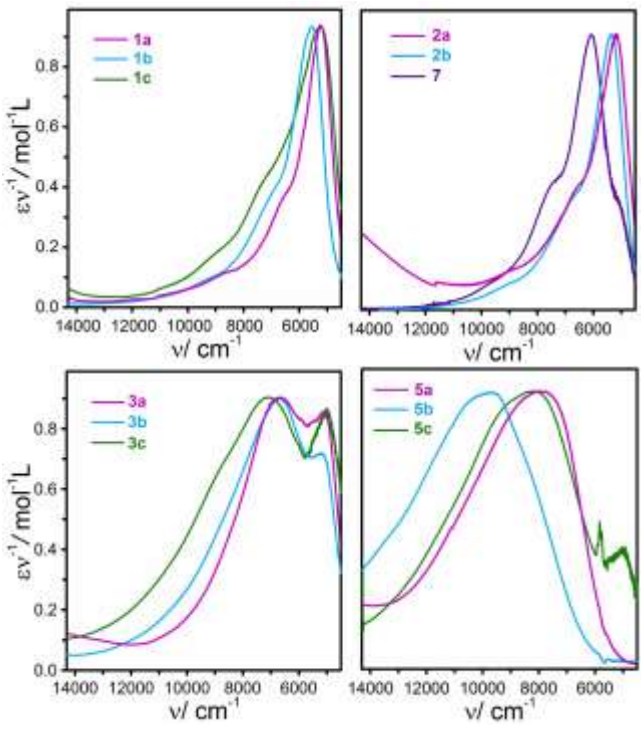

Figure 5. Normalized NIR spectra collected in THF solution for (top left) **1a – c**, (top right) **2a – b** and **7**, (bottom left) **3a – c**, and (bottom right) **5a – c**.

The NIR spectra of **1a** – **c** display very sharp, asymmetric, solvent-independent charge transfer bands which in THF solution are observed at 5200, 5535, and 5130 cm^{-1}, with vibrational overtones at higher energy that have average spacing of 1055, 1000, and 1016 cm^{-1}, respectively (Table S10, Figure 5, Figures S14-S16). We propose that the observed NIR bands in each of **1a** – **c** are intraligand π*- π* transitions. Complexes **2a** – **b** each contain two ligands with 1- charge (Scheme 2), and $(I_2P^{\cdot-})AlCl_2$ (**7**) was synthesized as an analog with a single monoanionic ligand (see SI for synthetic procedures). NIR spectra of **2a** – **b** show sharp bands observed in THF at 5150 and 5321 cm^{-1} with vibrational overtones at higher energy, and the spectrum of **7** likewise shows a sharp transition in THF at 6036 cm^{-1} (Table S10, Figures S17, S18). In all spectra, **1a** – **c**, **2a** – **b**, and **7**, vibronic coupling suggests that the orbital pathway for the transition is primarily ligand-based. Low energy NIR bands have been reported for π* - π* transitions in organic anion radicals. As an example, the spectrum of bis-indanone anion radical shows a sharp IVCT transition at 6290 cm^{-1},[34] and the spectrum of diquinone radical anion has a sharp transition at 6410 cm^{-1} assigned as π* - π* transition.[35] Electron delocalization has also been probed in nitrile-substituted organic anions where UV-Vis-NIR spectra show transitions in the visible range assigned as SOMO-1 to SOMO (or π - π*), and the NIR bands were assigned as SOMO to SOMO+1, i.e. π* - π* transitions.[36]

The NIR spectra of **3a** – **c** demonstrated broad solvent-independent bands observed in MeCN at 6850, 6695, and 7425 cm^{-1}, respectively (Figures 4, S19-S21), as well as narrower, solvent-independent bands at 5060, 5085, and 5080 cm^{-1}. Based on the discussion of **1a** – **c**, **2a** – **c**, and **7** we assign the narrow, lower energy bands as a π* - π* transitions on $I_2P^{\cdot-}$. Diamagnetic **4a** – **c**, containing two I_2P^{2-}

ligands, display no absorption bands in the NIR region, and the NIR spectra of **5a** – **c** (Figure S22) each contain one broad, asymmetric band observed at 7860, 9721 and 8250 cm^{-1}, respectively, in THF. Based on these comparisons, the broad bands observed for **3a** – **c** and **5a** – **c** involve both ligands in each molecule and are assigned as LLCT transitions. This is consistent with the CV (*vide supra*) and EPR spectroscopic data (*vide infra*).

Observed solvent independence is generally a clear indication of a Class III system whereas solvent dependence of $\Delta\nu_{max}$ is considered an indication of a Class II system because it arises from a dipole moment change accompanying the electron transfer event, or the reorganization energy needed to transfer an electron from one site to the other. Wherever possible, we collected NIR spectra in benzene, THF and MeCN which span a dielectric constant range of 34.3, as others have done.[1,10] Solubility of some compounds precluded data collection in benzene, and **5a** and **5b** were unstable in MeCN. Solvent independence, defined as $\Delta\nu_{max} < 200\ cm^{-1}$, was observed for all of the bands in **3a** and **3b** consistent with Class III behavior. For **3c** and **5c** $\Delta\nu_{max}$ are 325 and 820 cm^{-1}, respectively, and this supports their tentative assignment as Class II MV (Figure 6). We note that **3c** has OMe substituents of I_2P as *O*-donor ligands to the In center and these could be displaced by coordinating solvents such as THF to give an alternative origin for the solvent dependence. For example, the crystal structure of **4c** shows a six-coordinate, octahedral In center which is further evidence that the coordination of the OMe substituents can vary; therefore, it is possible that the observed solvent-dependence of the NIR bands in **3c** and **5c** stems from solvation-induced coordination sphere changes. This is discussed in more detail using EPR spectroscopic measurements below (*vide infra*).

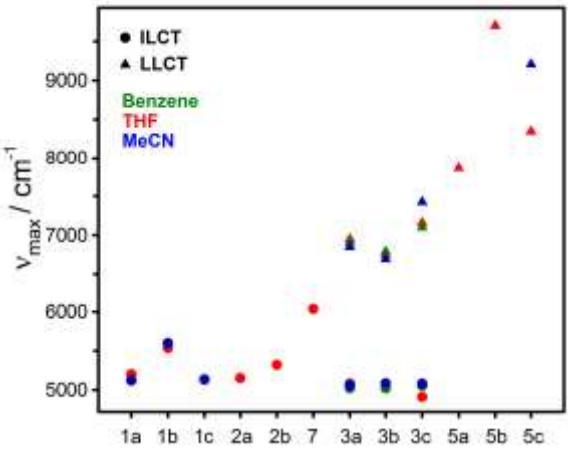

Figure 6. Comparison of ν_{max} of NIR absorption bands of **1a – c**, **2a – b**, **3a – c** and **5a** – **5b** in solvents spanning dielectric constant range of 34: benzene (ε = 2.28), THF (ε = 1.89), and MeCN (ε = 36.6).

In general, the energies of the broad bands described for each of **3a** – **c**, and **5a** – **c** shift to higher energy as compounds are successively reduced from $[(I_2P^{\cdot-})(I_2P^{2-})M]$ to $[(I_2P^{2-})(I_2P^{3-})M]^{2-}$. We speculate that this shift arises from the increased energy necessary for electron transfer to take place as the ligands contain more negative charge. It has been generally discussed that when absorption bands have $\Delta\nu_{1/2} < 2000\ cm^{-1}$, $\varepsilon_{max} > 5000\ M^{-1}cm^{-1}$, and are solvent-independent the compounds are most likely Class III.[36,37] Based on that simple definition, the transitions of **3a – b** can be tentatively assigned as characteristic of Class III, **3c** is Class II/III, and **5a – c** are Class II. Further analysis of these assignments follows.

Further Analysis of NIR spectra. To further understand the NIR spectra of **3a – c** and **5a – c**, a more detailed analysis of the absorption bands observed in the NIR spectra was performed using three classical methods to calculate parameters associated with the extent of electronic coupling. The multiple Gaussian distributions in each spectra were deconvoluted using non-linear least square (NLS) analysis in R so that the band peak maximum (ν_{max}), molar absorptivity (ε_{max}), and full width at half-maximum ($\Delta\nu_{1/2}$) could be obtained (see SI for full details, Figures S14 – S22).

The Hush model (equation S3) affords an electronic coupling parameter (denoted as H_{ab1} in Table 4).[37,38] This method is most accurate for weakly interacting Class II systems with Gaussian-shaped bands, and often severely underestimates a true H_{ab1}. Calculation of H_{ab1} also relies on accurate determination of *r*, and this is inaccurate using metrics obtained from solid-state structures.[39] In the series **1** – **5**, we take *r* to be the N_{py}-N_{py}' distance between the bis(imino)pyridine ligands.[40] In a second approach, the Brunschwig and Sutin method (equations S4, S5) was used to calculate electronic coupling (H_{ab2} in Table 4) (Table S11).[41] It is known that this method often over-estimates electronic coupling. A third approach employed the parameter Γ which is obtained from comparison of the experimentally determined band width, $\Delta\nu_{1/2}$, and calculated value $\Delta\nu_{1/2}^{o}$ (eq S6-S7). Experimental values of $\Delta\nu_{1/2}$ that are lower than calculated $\Delta\nu_{1/2}$ are indicative of Class III systems, whereas Class II systems exhibit experimental values 30-40% in excess of the calculated $\Delta\nu_{1/2}^{o}$.[42] More specifically, for Class II systems, Γ < 0.5; and for Class III systems, Γ > 0.5.[43] Based on the detailed analysis of the NIR spectra along with the considerations such as solvent dependence of the bands and electrochemical data, we conclude that **3a** – **b** are Class III MV, **3c** is Class II/III, and **5a** – **c** are Class II.

Electron Paramagnetic Resonance Spectroscopy. EPR spectroscopy measurements were performed on samples of the biradical complexes **2a** – **b**, and MV **3a** – **c**. EPR and NIR spectroscopic measurements operate over the time domain 10^{-7} - 10^{-10}, and 10^{-11} - 10^{-14} s, respectively, and so for modestly coupled systems charge states can appear averaged on the EPR time scale.[44] Furthermore, some of the EPR and all of the ENDOR spectra were collected on frozen samples which may introduce apparent reduction in electronic coupling compared with the NIR data.

Table 4. Absorption band analysis (ν_{max}, ε_{max}, $\Delta\nu_{1/2}$), electronic couplings (H_{ab1} and H_{ab2}), and Γ for **3a – c** and **5a – c**.

	Solvent	ν_{max} (cm^{-1})	ε_{max} (M^{-1} cm^{-1})	$\Delta\nu_{1/2}$ (expt) (cm^{-1})[d]	$\Delta\nu_{1/2}$ (calc)[a] (cm^{-1})	H_{ab1} (cm^{-1})[b]	H_{ab2} (cm^{-1})[c]		Γ[d]
3a	MeCN	6850	4950	2574	3978	1610	4640	(4860)	0.35
	THF	6950	5110	2410	4007	1590	4680	(4880)	0.40
	Benzene	6909	6800	2279	3995	1780	4660	(4870)	0.43
3b	MeCN	6695	4020	2808	3932	1460	4410	(4580)	0.29
	THF	6750	2940	2527	3948	1190	4430	(4600)	0.36
	Benzene	6790	1630	2691	3960	915	4440	(4610)	0.32
3c	MeCN	7425	1520	3276	4141	967	4390	(4450)	0.21
	THF	7159	2690	3393	4066	1280	4310	(4380)	0.17
	Benzene	7100	1190	2972	4050	797	4290	(4370)	0.27
5a[e]	THF	7860	3770	6318	4261	2350	4400	(4420)	-0.48
5b[e]	THF	9721	3400	6377	4738	2430	5100	(5110)	-0.35
5c[e]	MeCN	9210	7470	5520	4612	3100			-0.34
	THF	8350	3430	5733	4392	2040			-0.41

[a] Calculated from eq S7. [b] Calculated from eq S3. [c] Using free energy of comproportionation reaction for weakly coupled (and strongly coupled) system, eq S4 and S5. [d] Calculated from eq S6. [e] Generated *in situ*.

The 60 K X-band continuous wave (cw) EPR spectrum of the dilute frozen solution of **2a** features flanking shoulders between 310 and 365 mT, assigned to the Δm_S ± 1 transitions characteristic of a triplet state (S = 1). The spectrum of **2b** features a set of Δm_S = ±1 peaks centered at 320 and 350 mT. The spectra of both **2a** and **2b** show the expected weak Δm_S = ±2 transition at half-field, 165 mT (Figure 7), which confirms that **2a** – **b** have biradical electronic states that can be populated at low temperatures. A strong central line assigned to a doublet species (S = ½) is also observed, and is likely generated from trace dioxygen contamination, as observed in a related study.[17a] The signals arising from **2a** and **2b** are centered at 335 mT, g = 2.004 and 333 mT, g = 2.005, respectively, and have small deviations from g_e, indicative of carbon- or nitrogen-based radicals. Based on a simple dipole approximation obtained from D and extracted from simulation of S = 1 ground state (See SI, Experimental Section), the radicals are closer in space in **2b**, compared to **2a**, although the crystallographic distance between ligands is greater in **2b**. The change in temperature corrected signal intensity was modeled and provided an estimate for the ferromagnetic exchange coupling for **2a** and **2b** as J = 56 and 35 cm^{-1}, respectively (Figure S23). The decrease in J coupling from **2a** to **2b** represents the sum of all coupling pathways and may arise from an increase in the magnitude of the antiferromagnetic coupling relative to the magnitude of the ferromagnetic interaction rather than a decreased overall exchange interaction.

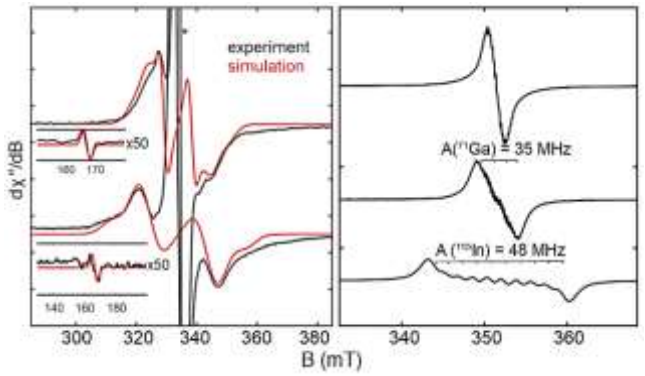

Figure 7. (left) X-band cw EPR spectra of a frozen solution of 1 mM **2a** (top) and **2b** (bottom) in THF. Insets: corresponding half field transitions. (right) X-band cw EPR spectra at 298 K of 1 mM **3a** (top), **3b** (middle), and **3c** (bottom) in toluene. * is signal from **3a – b** (Figure S24). Experimental parameters given in the Experimental Section of the SI.

Solution phase X-band EPR performed on samples of **3a – c** in toluene at 298 K confirm a ligand based radical (Figure 7 right). **3a** and **3b** have a 20-line peak pattern separated by 6 MHz, which we assign as ligand ^{14}N or ^{1}H hyperfine interaction (Figure S25, S26). The spectra of **3b** and **3c** feature a central 5-line and 10-line pattern, respectively, with coupling constants of 35 and 48 MHz assigned to ^{69}Ga (I = 3/2) or ^{115}In (I = 9/2). This indicates that the ligand electron delocalization is largely unchanged at room temperature between **3a** and **3b**. X-band cw EPR data for **3a** was not sufficiently resolved and so Q-band pulsed ENDOR spectra collected at 40 K were used to probe the ^{27}Al and ^{1}H hyperfine interactions (Figure S27 - 28). No signals for Ga or In were observed in the ENDOR spectra of **3b** and **3c**. From the small (T ≈ 3 MHz) anisotropy of the ^{27}Al hyperfine interaction, or the isotropic component of that spectrum 0.03 electrons reside in the Al p-orbitals of **3a**

(Tables S12 - S14).[45] For **3b** and **3c** cw EPR spectra indicate that 0.0029 and 0.0024 electrons are localized at Ga and In, respectively (Figure 7 right, Table S14, eq S8-S9).

The proton region of the ENDOR spectra collected at 40 K have the same splitting pattern in **3a**, **3b**, and **7**, and the relative ^{1}H hyperfine interactions are consistent with a greater degree of delocalization of the electron in **3a** and **3b** as compared with **7** (Figure S28 – S29, Table 5, Table S13). That data suggests a partial delocalization of the electron at 40 K on the EPR timescale, and this is not inconsistent with the full Class III delocalization characterized at 298 K on the time scale of NIR spectroscopic measurements. ^{1}H hyperfine, as detected from ENDOR experiments, decreases ~ 40% in **3c** compared with **3a** and **3b**. This could be attributed to the lower symmetry at In and potential for delocalization onto additional solvent or methoxy ligands coordinated to the In center. Possible solvent dependence of the coordination spheres of **3a** – **c** was probed by collecting cw EPR spectra in toluene and THF at 40 K (Figure S30). The spectrum of **3c** in toluene can be simulated well with parameters that follow the trend of **3a** and **3b** but hyperfine splittings observed for **3c** in THF could not be simulated simply with In hyperfine. Spectra of **3a** – **b** are the same in THF and toluene. This indicates that the SOMO of **3c** is substantially changed under different solvation conditions, and these observed solvation effects suggest that the solvent dependence of the NIR spectra observed for **3c** may arise from coordination sphere changes at In rather than as an effect of the solvent dielectric constant. EPR or ENDOR analyses of **5a** – **c** were not performed since those compounds lack sufficient stability when handled over extensive periods.

Table 5. ^{1}H hyperfine coupling a_{iso} (MHz) determined from frozen solutions of toluene at 60 K. [a]

3a	3b	3c	7
[4.5 1.7 1.3] [11.5 11 10.5] [18 18 9]	[4.5 1.7 1.3] [11.5 11 10.5] [18 18 9]	[4 2.2 1.0] [5 3.5 3.5] [7 7 10]	[4.5 1.7 1.3] [14 13 12] [21.5 21 9]

[a] Determined by Q-band Davies ENDOR at 60 K centered about the ^{1}H larmor frequency.

Summary. Taken together the results of NIR band analyses, including $\Delta\nu_{1/2}$ < 2000 cm^{-1}, solvent independent ν_{max}, Γ parameters, and deviation of NIR band shapes from Gaussian, suggest that the NIR absorption bands observed for **3a** – **b** arise from a Class III full delocalization. Electrochemical data (K_c values) and EPR analyses support this assessment. Broad and weak NIR transitions, $\Delta\nu_{1/2}$ > 2000 cm^{-1} and ε_{max} < 5000 M^{-1}cm^{-1}, along with solvent dependence of ν_{max} suggest that **3c**, and **5a** – **c** fall within the definition of Class II, although the high asymmetry in the NIR band for **3c** suggests that Class II/III borderline is more accurate. Solvation-induced coordination sphere changes observed by EPR spectroscopy likely contribute to the observed solvent dependence of the NIR signatures of **3c**. Attenuation of the electron delocalization as more electrons are added to the ligands, as in **5a** – **c**, compared with **3a** – **c** is reasonably attributed to the increased charge of the ligands in more reduced complexes. IL transitions on the ligands with 1- charge in **1a** – **c**, **2a** – **c**, and **3a** – **c** are all assigned as π* - π* transitions.

Almost ideal octahedral coordination geometry is credited with the observed Class III behavior in the MV systems **3a** and **3b**, and the attenuated Class II/III assignment in **3c** is consistent with the lower symmetry about the In ion that can accommodate additional ligands to span solvent-dependent 6 – 8 coordination. The assessment of geometry as an important factor promoting the delocalized structure of **3a** and **3b** is supported by the absence of electronic coupling and electron delocalization between radical ligands connected by Group 13 ions with trigonal bipyramidal coordination geometry.[17,18] We propose that the octahedral coordination geometry is necessary to accommodate efficient orbital overlap necessary for electronic coupling with the valence *p*-orbitals of the Group 13 ions. Further attenuation of electron delocalization in **5a** – **c**, which are assigned as Class II most likely arises from higher population of the ligand π* orbitals with higher anionic charge on the compounds.

Parameters other than coordination sphere geometry in the rationalization of the data were also considered. As an example, the distance between radical sites, defined as *r* in the Hush model, increases in the order Al, Ga, In where ionic radii are 54, 62, and 80 Å, respectively, and so a dependence on *r* is predicted to be a gradual attenuation in the electronic coupling on moving from Al to Ga and then to In.[46] However, the observed results are that electronic coupling is similar for Al- and Ga-bridged ligands, and lower for In complexes. Alternatively, the relative reduction potentials of the Group 13 ions predict weaker electronic coupling for Al complexes relative to the coupling mediated by Ga or In. However, it is the Al and Ga complexes, **3a** and **3b**, that demonstrate Class III behavior compared with **3c** that falls in the Class II/III borderline.

The series characterized here also includes **2a** and **2b** which each have two ligands in 1- charge states, with radicals that are ferromagnetically coupled, with J = 55 and 35 cm^{-1}, respectively. Compounds **4a** – **c** are diamagnetic, and **6a** contains two ligands in 3- charge states that were isolated at low temperature and characterized crystallographically.

CONCLUSIONS

Water stable organic MV compounds have been prepared spanning five charge states including three that are MV states (Chart 2). The electronic coupling between ligand end groups is modulated by oxidation and reduction of the ligands with electron delocalization observed for [(I_2P^-)(I_2P^{2-})M], and when M = Al or Ga. The analogous In^{III} compounds have solvent-dependent coordination geometry and that lowered symmetry supports Class II/III behavior. Further-reduced MV compounds, [(I_2P^{2-})(I_2P^{3-})M] are assigned as Class II for M is Al, Ga, or In.

These examples show us that octahedral coordination geometry provides an orbital pathway to support electron delocalization between radical ligands that are connected by metal ions with valence *p*-orbitals, as in Group 13. In this series of compounds Al facilitates stronger electronic coupling than either Ga or In, and the electronic coupling is greatest when the overall molecular charge is lowest and fewer electrons populate the ligand π* framework.

ASSOCIATED CONTENT

SUPPORTING INFORMATION

Crystallographic information (CIF)
Experimental details, tables summarizing X-ray structural data, fits to NIR spectra, electrochemical measurements in THF, calculation of electronic coupling parameters, EPR spectroscopic measurements (PDF).
The Supporting Information is available free of charge on the ACS Publications website.

AUTHOR INFORMATION

Corresponding Author

* e-mail: laberben@ucdavis.edu

Author Contributions

The manuscript was written through contributions of all authors.

ACKNOWLEDGMENT

Synthesis and characterization of compounds was supported by the National Science Foundation with award CHE-1763821; characterization of mixed-valent Ga and In compounds was supported by the Office of Naval Research NEPTUNE program with award N000141712811. RDB thanks The National Science Foundation Center for Chemical Innovation (CHE-1305124) for support. The National Science Foundation also provided the dual-source X-ray diffractometers (Grants CHE-0840444 and CHE-1531193). We thank Drs. A. J. Moule and S. M. Kauzlarich for use of UV-Vis-NIR spectrometers, and C. D. Arnold for assistance with R.

REFERENCES

[1] Canzi, G.; Goeltz, J. C.; Henderson, J. S.; Park, R. E.; Maruggi, C.; Kubiak, C. P. On the Observation of Intervalence Charge Transfer Bands in Hydrogen-Bonded Mixed-Valence Complexes. *J. Am. Chem. Soc*. **2014**, *136*, 5, 1710-1713.

[2] Wang, B.; Zheng, S.; Saha, S.; Bao, L.; Lu, X.; Guldi, D.M. Understanding Charge-Transfer Characteristics in Crystalline Nanosheets of Fullerene/(Metallo)porphyrin Cocrystals. *J. Am. Chem. Soc*. **2017**, *139*, 10578−10584.

[3] Hua, C.; Doheny, P. W.; Ding, B.; Chan, B.; Yu, M.; Kepert, C. J.; D'Alessandro, D. M. Through-Space Intervalence Charge Transfer as a Mechanism for Charge Delocalization in Metal-Organic Frameworks. *J. Am. Chem. Soc*. **2018**, *140*, 6622−6630.

[4] (a) Peeks, M. D.; Tait, C. E.; Neuhaus, P.; Fischer, G. M.; Hoffmann, M.; Haver, R.; Cnossen, A.; Harmer, J. R.; Timmel, C. R.; Anderson, H. L. Electronic Delocalization in the Radical Cations of Porphyrin Oligomer Molecular Wires. *J. Am. Chem. Soc*. **2017**, *139*, 10461−10471. (b) Olivier, C.; Kim, B.; Touchard, D.; Rigaut, S. Redox-Active Molecular Wires Incorporating Ruthenium(II) σ-Arylacetylide Complexes for Molecular Electronics. *Organometallics*, **2008**, *27*, 509-518.

[5] Parthey, M.; Kaupp, M., Quantum-chemical insights into mixed-valence systems: within and beyond the Robin-Day scheme. *Chem. Soc. Rev.* **2014,** *43* (14), 5067-5088.

[6] a) Zhu, C.; Ji, X.; You, D.; Chen, T. L.; Mu, A. U.; Barker, K. P.; Klivansky, L. M.; Liu, Y.; Fang, L. B←N Coordination Promoted Delocalization and Hyperconjugation Lead to Extraordinary Redox Activities in Ladder-Type Conjugated Molecules. *J. Am. Chem. Soc.* **2018**, *140*, 18173-18182. b) Tichnell, C. T.; Daley, D. R.; Stein, B. W.; Shultz, D. A.; Kirk, M. L.; Danilov, E. O. Wave Function Control of Charge-Separated Excited-State Lifetimes. *J. Am. Chem. Soc.* **2019**, *141*, 3986-3992.

[7] a) Mani, T.; Grills, D. C.; Newton, M. D.; Miller, J. R. Electron Localization of Anions Probed by Nitrile Vibrations. *J. Am. Chem. Soc.* **2015**, *137*, 10979−10991. b) Grozema, F. C.; van Duijnen, P. T.; Berlin, Y. A.; Ratner, M. A.; Siebbeles, L. D. A. Intramolecular Charge Transport along Isolated Chains of Conjugated Polymers: Effect of Torsional Disorder and Polymerization Defects, *J. Phys. Chem. B* **2002**, *106*, 7791. c) Bredas, J. L.; Beljonne, D.; Coropceanu, V.; Cornil, J. Charge-Transfer and Energy-Transfer Processes in π-Conjugated Oligomers and Polymers: A Molecular Picture. *Chem. Rev*. **2004**, *104*, 4971.

[8] Hansmann, M. M.; Melaimi, M.; Bertrand, G., Organic Mixed Valence Compounds Derived from Cyclic (Alkyl)(amino)carbenes. *J. Am. Chem. Soc.* **2018,** *140* (6), 2206-2213.

[9] Creutz, C.; Taube, H., Direct approach to measuring the Franck-Condon barrier to electron transfer between metal ions. *J. Am. Chem. Soc.* **1969,** *91* (14), 3988-3989.

[10] Hernández Sánchez, R.; Zheng, S.-L.; Betley, T. A., Ligand Field Strength Mediates Electron Delocalization in Octahedral $[(HL)_0Fe_6(L')_m]^{n+}$ Clusters. *J. Am. Chem. Soc.* **2015,** *137* (34), 11126-11143.

[11] Zhang, J.; Chen, Z.; Yang, L.; Pan, F.-F.; Yu, G.-A.; Yin, J.; Liu, S. H., Elaborately Tuning Intramolecular Electron Transfer Through Varying Oligoacene Linkers in the Bis(diarylamino) Systems. *Sci. Rep.* **2016,** *6*, 36310.

[12] (a) Bonvoisin, J.; Launay, J.-P.; Rovira, C.; Veciana, J. Purely Organic Mixed-Valence Molecules with Nanometric Dimensions Showing Long-Range Electron Transfer. Synthesis, and Optical and EPR Studies of a Radical Anion Derived from a Bis(triarylmethyl)Diradical. *Angew. Chem., Int. Ed. Engl*. **1994**, *33*, 2106-2109. (b) Rovira, C.; Ruiz-Molina, D.; Elsner, O.; Vidal-Gancedo, J.; Bonvoisin, J.; Launay, J.-P.; Veciana, J. Influence of Topology on the Long-Range Electron-Transfer Phenomenon. *Chem. - Eur. J*. **2001**, 7, 240-250.

[13] (a) Rosokha, S. V.; Sun, D. L.; Kochi, J. K. Conformation, Distance, and Connectivity Effects on Intramolecular Electron Transfer between Phenylene-Bridged Aromatic Redox Centers. *J. Phys. Chem. A.* **2002**, *106*, 2283-2292. (b) Lambert, C.; Nöll, G., The Class II/III Transition in Triarylamine Redox Systems. *J. Am. Chem. Soc.* **1999,** *121* (37), 8434-8442.

[14] (a) Jones, S. C.; Coropceanu, V.; Barlow, S.; Kinnibrugh, T.; Timofeeva, T.; Brédas, J.-L.; Marder, S. R., Delocalization in Platinum−Alkynyl Systems: A Metal-Bridged Organic Mixed-Valence Compound. *J. Am. Chem. Soc.* **2004,** *126* (38), 11782-11783. (b) Yao, C-J.; Yao, J.; Zhong, Y-W. Electronic Communication between Two Amine Redox Centers Bridged by a Bis(terpyridine)ruthenium(II) Complex. *Inorg. Chem*. **2011**, *50*, 6847-6849. (c) Ray, K.; Petrenko, T.; Wieghardt, K.; Neese, F. Joint spectroscopic and theoretical investigations of transition metal complexes involving non-innocent ligands. *Dalton Trans*., **2007**, 1552-1566. (d) Kojima, T.; Ogishima, F.; Nishibu, T.; Kotani, H.; Ishizuka, T.; Okajima, T.; Nozawa‖, S.; Shiota, Y.; Yoshizawa, K.; Ohtsu, H.; Kawano, M.; Shiga, T.; Oshio, H. Intermediate-Spin Iron(III) Complexes Having a Redox-Noninnocent Macrocyclic Tetraamido Ligand. *Inorg. Chem*. **2018**, *57* (16), 9683-9695.

[15] Hewage, J. S.; Wanniarachchi, S.; Morin, T. J.; Liddle, B. J.; Banaszynski, M.; Lindeman, S. V.; Bennett, B.; Gardinier, J. R., Homoleptic Nickel(II) Complexes of Redox-Tunable Pincer-type Ligands. *Inorg. Chem.* **2014,** *53* (19), 10070-10084.

[16](a) Lu, C. C.; Bill, E.; Weyhermuller, T.; Bothe, E.; Wieghardt, K. Neutral Bis(α-iminopyridine)metal Complexes of the First-Row Transition Ions (Cr, Mn, Fe, Co, Ni, Zn) and Their Monocationic Analogues: Mixed Valency Involving a Redox Noninnocent Ligand System. *J. Am. Chem. Soc.* **2008,** *130*, 3181-3197. (b) de Bruin, B.; Bill, E.; Bothe, E.; Weyhermüller, T.; Wieghardt, K., Molecular and Electronic Structures of Bis(pyridine-2,6-diimine)metal Complexes $[ML_2](PF_6)n$ (n = 0, 1, 2, 3; M = Mn, Fe, Co, Ni, Cu, Zn). *Inorg. Chem.* **2000,** *39* (13), 2936-2947. (c) Scarborough, C. C.; Lancaster, K. M.; DeBeer, S.; Weyhermüller, T.; Sproules, S.; Wieghardt, K. Experimental Fingerprints for Redox-Active Terpyridine in $[Cr(tpy)_2](PF_6)_n$ (n = 3−0), and the Remarkable

Electronic Structure of $[Cr(tpy)_2]^{1-}$. *Inorg. Chem*. **2012**, *51*, 3718-3732.

[17] a) Myers, T. W.; Kazem, N.; Stoll, S.; Britt, R. D.; Shanmugam, M.; Berben, L. A., A Redox Series of Aluminum Complexes: Characterization of Four Oxidation States Including a Ligand Biradical State Stabilized via Exchange Coupling. *J. Am. Chem. Soc.* **2011,** *133* (22), 8662-8672. b) Myers, T. W.; Berben, L. A., Countercations Direct One- or Two-Electron Oxidation of an Al(III) Complex and Al(III)–Oxo Intermediates Activate C–H Bonds. *J. Am, Chem. Soc.* **2011,** *133* (31), 11865-11867. c) Kowolik, K.; Shanmugam, M.; Myers, T. W.; Cates, C. D.; Berben, L. A., A redox series of gallium(iii) complexes: ligand-based two-electron oxidation affords a gallium-thiolate complex. *Dalton Trans.* **2012,** *41* (26), 7969-7976. d) Cloke, F. G. N.; Dalby, C. I.; Daff, P. J.; Green, J. C. Electronic Structure and Photoelectron Spectroscopy of $Al(Me_3CNCHCHNCMe_3)_2$ and $Ga\ Me_3CNCHCHNCMe_3)_2$. *J. Chem. Soc., Dalton Trans*., **1991**, 181-184.

[18] Liddle, B. J.; Wanniarachchi, S.; Hewage, J. S.; Lindeman, S. V.; Bennett, B.; Gardinier, J. R., Electronic Communication Across Diamagnetic Metal Bridges: A Homoleptic Gallium(III) Complex of a Redox-Active Diarylamido-Based Ligand and Its Oxidized Derivatives. *Inorg. Chem.* **2012,** *51* (23), 12720-12728.

[19] (a) Dunn, T. J.; Chiang, L.; Ramogida, C. F.; Hazin, K.; Webb, M. I.; Katz, M. J.; Storr, T. Class III Delocalization and Exciton Coupling in a Bimetallic Bis-ligand Radical Complex. *Chem. Eur. J*. **2013**, *19*, 9606–9618. (b) Lyons, C. T.; Stack, T. D. P. Recent advances in phenoxyl radical complexes of salen-type ligands as mixed-valent galactose oxidase models. *Coord. Chem. Rev*. **2013**, *257*, 528-540. (c) Kurahashi, T.; Fujii, H. One-Electron Oxidation of Electronically Diverse Manganese(III) and Nickel(II) Salen Complexes: Transition from Localized to Delocalized Mixed-Valence Ligand Radicals. *J. Am. Chem. Soc*. **2011**, *133*, 8307–8316.

[20] Myers, T. W.; Sherbow, T. J.; Fettinger, J. C.; Berben, L. A., Synthesis and characterization of bis(imino)pyridine complexes of divalent Mg and Zn. *Dalton Trans.* **2016,** *45* (14), 5989-5998.

[21] (a) Cladis, D. P.; Kiernicki, J. J.; Fanwick, P. E.; Bart, S. C., Multi-electron reduction facilitated by a trianionic pyridine(diimine) ligand. *Chem. Commun.* **2013,** *49* (39), 4169-4171. (b) Enright, D.; Gambarotta, S.; Yap, G. P. A.; Budzelaar, P. H. M., The Ability of the α,α′-Diiminopyridine Ligand System to Accept Negative Charge: Isolation of Paramagnetic and Diamagnetic Trianions. *Angew. Chem. Int. Ed.* **2002,** *41* (20), 3873-3876. (c) Tondreau, A. M.; Stieber, S. C. E.; Milsmann, C.; Lobkovsky, E.; Weyhermüller, T.; Semproni, S. P.; Chirik, P. J. Oxidation and Reduction of Bis(imino)pyridine Iron Dinitrogen Complexes: Evidence for Formation of a Chelate Trianion. *Inorg. Chem.* **2013,** *52* (2), 635-646. (d) Anderson, N. H.; Odoh, S. O.; Yao, Y.; Williams, U. J.; Schaefer, B. A.; Kiernicki, J. J.; Lewis, A. J.; Goshert, M. D.; Fanwick, P. E.; Schelter, E. J.; Walensky, J. R.; Gagliardi, L.; Bart, S. C. Harnessing redox activity for the formation of uranium tris(imido) compounds. *Nat. Chem.* **2014,** *6* (10), 919-926. (e) Anderson, N. H.; Odoh, S. O.; Williams, U. J.; Lewis, A. J.; Wagner, G. L.; Lezama Pacheco, J.; Kozimor, S. A.; Gagliardi, L.; Schelter, E. J.; Bart, S. C. Investigation of the Electronic Ground States for a Reduced Pyridine(diimine) Uranium Series: Evidence for a Ligand Tetraanion Stabilized by a Uranium Dimer. *J. Am. Chem. Soc*., **2015**, *137*, 4690–4700.

[22] Römelt, C.; Weyhermüller, T.; Wieghardt, K. Structural characteristics of redox-active pyridine-1,6-diimine complexes: Electronic structures and ligand oxidation levels. *Coord. Chem. Rev.* **2019,** *380*, 287-317.

[23] a) Myers, T. W.; Berben, L. A. Aluminum-Ligand Cooperative N-H Bond Activation and an Example of Dehydrogenative Coupling. *J. Am. Chem. Soc*. **2013**, *135*, 9988-9990. b) Thompson, E .J.; Berben, L. A. Electrocatalytic Hydrogen Production by an Aluminum(III) Complex: Ligand-Based Proton and Electron Transfer. *Angew. Chem. Intl. Ed*. **2015**, *54*, 11642-11646.

[24] Thompson, E. J.; Myers, T. W.; Berben, L. A. Synthesis of Square Planar Aluminum(III) Complexes. *Angew. Chem.* **2014**, *53*, 14132-14134.

[25] Cooper BF, Macdonald CL. (1,4,7,10,13,16-Hexaoxacyclo-octadeca-ne)dimethyl-indium(III) trifluoro-methane-sulfonate. *Acta Crystallogr Sect E Struct Rep Online*. **2011**, *67*, 233-234.

[26] Ahlrichs, R.; Eichhöfer, A.; Fenske, D.; Hampe, O.; Kappes, M. M.; Nava, P.; Olkowska-Oetzel, J. Synthesis and Structure of $[Ag_{26}In_{18}S_{36}Cl_6(dppm)_{10}(thf)_4][InCl_4(thf)]_2$ — A Combined Approach of Theory and Experiment. *Angew. Chem. Int. Ed*. **2004**, 43, 3823-3827.

[27] Schnitter, C.; Waezsada, S. D.; Roesky, H. W. Teichert, M.; Uso´n, I.; Parisini, E. Synthesis and Characterization of (4-Fluorophenyl)amino-Based Amino- and Iminometallanes of Group 13. Crystal Structures of $(MeAlNR_f)_4$, $(MeMNR_f)_6 \bullet n$THF (M = Al, n = 2; M = Ga, n = 7), and $(MeIn(THF)NR_f)_4$ (R_f = 4-C_6H_4F). *Organometallics*. **1997**, *16*, 1197-1202.

[28] Thompson, E. J.; Myers, T. W.; Berben, L. A. Synthesis of Square-Planar Aluminum(III) Complexes. *Angew. Chem. Intl. Ed.* **2014**, *53*, 14132-14134.

[29] Oehman, L. O. Equilibrium and structural studies of silicon(IV) and aluminum(III) in aqueous solution. 17. Stable and metastable complexes in the system hydrogen (+)-aluminum(3+)-citric acid. *Inorg. Chem.* **1988,** *27* (15), 2565-2570.

[30] Myers, T. W.; Berben, L. A. Aluminum–Amido-Mediated Heterolytic Addition of Water Affords an Alumoxane. *Organometallics.* **2013,** *32* (22), 6647-6649.

[31] Ivanov, M. V.; Wadumethrige, S. H.; Wang, D.; Rathore, R. Unraveling the Coulombic Forces in Electronically Decoupled Bichromophoric Systems during Two Successive Electron Transfers. *Chem. Eur. J*. **2017**, *23*, 8834-8838.

[32] Creutz, C.; Chou, M. H., Solvent dependences of spectral and redox properties of pyrazine (pz) complexes of ruthenium and osmium pentaammines: $Ru(NH_3)_5pzCH_3^{3+}$, $Os(NH_3)_5pzCH_3^{3+}$, and $[Ru(NH_3)_5]_2pz^{5+}$. *Inorg. Chem.* **1987,** *26* (18), 2995-3000.

[33] D'Alessandro, D. M.; Keene, F. R., Current trends and future challenges in the experimental, theoretical and computational analysis of intervalence charge transfer (IVCT) transitions. *Chem. Soc. Rev.* **2006,** *35* (5), 424-440.

[34] Schroeder, A. H.; Mazur, S. A Vibronic Model for Infrared Absorption by a Mixed Valence Anion Radical. *J. Am. Chem. Soc.* **1978**, *100* (23), 7339-7346.

[35] Almlöf, J. E.; Feyereisen, M. W.; Jozefiak, T. H.; Miller, L. L. Electronic Structure and Near-Infrared Spectra of Diquinone Anion Radicals. *J. Am. Chem. Soc*., **1990**, *112* (3) 1206-1214.

[36] Mani, T.; Grills, D. C.; Newton, M. D.; Miller, J. R. Electron Localization of Anions Probed by Nitrile Vibrations. *J. Am. Chem. Soc.* **2015,** *137*, 10979-10991.

[37] (a) Allen, G. C.; Hush, N. S. Intervalence-Transfer Absorption. Part 2. Theoretical Considerations and Spectroscopic Data. *Prog. Inorg. Chem*. **1967**, *8*, 357-389. (b) Robin, M. B.; Day, P. Mixed Valence Chemistry-A Survey and Classification. *Adv. Inorg. Chem. Radiochem*. **1968**, *10*, 247-422.

[38] Hush, N. S. Homogeneous and heterogeneous optical and thermal electron transfer. *Electrochim. Acta* **1968,** *13* (5), 1005-1023.

[39] a) Vance, F. W.; Karki, L.; Reigle, J. K.; Hupp, J. T.; Ratner, M. A. Aspects of Intervalence Charge Transfer in Cyanide-Bridged Systems: Modulated Electric Field Assessment of Distances, Polarizability Changes, and Anticipated First Hyperpolarizability Characteristics. *J. Phys. Chem. A.* **1998**, *102* (43) 8320-8324. b) Karki, L.; Lu, H. P.; Hupp, J. T. Electroabsorption Studies of Intervalence Charge Transfer in $(NC)_5FeCNOs(NH_3)^{5-}$: Experimental Assessment of Charge-Transfer Distance, Solvent Reorganization, and Electronic Coupling Parameters. *J. Phys. Chem. A.* **1996**, *100* (39), 15637-15639.

[40] Nelsen, S. F.; Tran, H. Q.; Nagy, M. A., Comparison of V Values for Some Nitrogen- and Metal-Centered π-Bridged Mixed-Valence Compounds. *J. Am. Chem. Soc.* **1998,** *120* (2), 298-304.

[41] Brunschwig, B. S.; Sutin, N., Energy surfaces, reorganization energies, and coupling elements in electron transfer. *Coord. Chem. Rev.* **1999,** *187* (1), 233-254.

[42] Creutz, C. Mixed Valence Complexes of d^5-d^6 Metal Centers. In *Prog. Inorg. Chem*., **1983**, *30*, 1-73.

[43] Brunschwig, B. S.; Creutz, C.; Sutin, N. Optical transitions of symmetrical mixed-valence systems in the Class II–III transition regime. *Chem. Soc. Rev*. **2002**, *31*, 168-184.

[44] a) McCusker, J. K.; Jang, H. G.; Zvagulis, M.; Ley, W.; Drickamer, H. G.; Hendrickson, D. N. Valence Trapping of Mixed-Valence $[Fe_3O(O_2CCH_3)_6(py)_3]$*S (S = Solvent) Complexes at High Pressure. *Inorg. Chem*. **1991**, *30* (9), 1985-1990. b) Mashuta, M. S.; Webb, R. J.; McCusker, J. K.; Schmitt, E. A.; Oberhausen, K. J.; Richardson, J. F.; Buchanan, R. M.; Hendrickson, D. N. Electron Transfer in $Fe^{II}Fe^{III}$ Model Complexes of Iron-Oxo Proteins. *J. Am. Chem. Soc*. **1992**, *114*, 3815-3827.

[45] Morton, J. R.; Preston, Atomic Parameters for Paramagnetic Resonance Data, K. F. *J. Mag. Res*. **1978**, *30*, 577-582.

[46] Housecroft, C. E.; Sharpe, A. G. *Inorganic Chemistry*, 4th ed.; Pearson: Harlow, 2007.

TOC Graphic

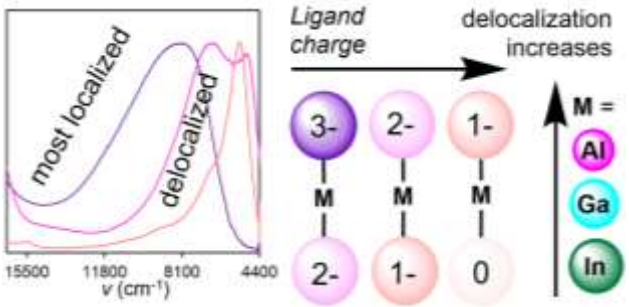
most localized
delocalized
15500
11800
8100
4400
ν (cm-1)
Ligand charge
delocalization increases
3-
2-
1-
M
M
M
2-
1-
0
M =
Al
Ga
In